Brushless DC Motor Characterisation and Selection for a Fixed Wing UAV

Darren Lance Gabriel
Department of Electrical and Electronic Engineering
University of Johannesburg
Johannesburg, South Africa

Johan Meyer
Department of Electrical and Electronic Engineering
University of Johannesburg
Johannesburg, South Africa

Francois du Plessis
Department of Electrical and Electronic Engineering
University of Johannesburg
Johannesburg, South Africa

***Abstract*—The aim of the paper is to present a method for evaluating brushless DC motors (BLDC) for fixed wing Unmanned Aerial Vehicles (UAVs). Selection of a BLDC motor, which operates in its efficient region for a UAV platform's specifications, will affect the endurance capabilities of the UAV platform. A four-constant model is presented as a means of modelling and predicting the characteristics of BLDC motors. Further, physical testing of each motor is performed on a constructed motor test bench. Validation of the model's results is compared to physical testing. The methods presented provide a means of accurately characterising a given BLDC motor. This data can be used to design the additional components used in the UAV's propulsion system.**

I. Introduction

The Unmanned Aerial Vehicle market has grown into a multi-billion dollar industry, with the UAV market worth over $4.9 billion in 2010 — largely due to the growing application domain for UAVs [1]. A UAV is an aircraft without an on-board human pilot. Instead the aircraft may be piloted remotely or using an autopilot system. Emerging applications in South Africa require UAVs to operate for long uninterrupted durations — typically between than 4 and 24 hours. Some of these applications include:

- Wildlife tracking;
- Traffic monitoring;
- Border patrols;
- Environmental research;
- Geographical mapping; and
- Numerous military applications

The above mentioned applications need to be performed with a UAV which, is "invisible" to the application for which it is used. Military reconnaissance for instance would benefit from a platform with low heat and noise signatures in the quest for "invisibility" to an enemy target. Data obtained from environmental research of atmospheric gases may be compromised, should the UAV platform produce gases from an internal combustion type propulsion system. Taking these aspects and the application domain into account, electrical propulsion becomes a better means of propulsion — over internal combustion engines [2]. Electric propulsion systems produce zero gaseous emissions, low heat, and generate less audible noise than a internal combustion system.

Realising long endurance flight requires, in addition to a high energy density power source, an efficient propulsion system. An electric propulsion system converts electrical energy to mechanical thrust, and consists of four main components: an electrical power source, Electronic Speed Controller (ESC), electric motor and a propeller (Fig. 1). Each of these components has their own performance characteristics and regions of maximum efficiency. The selection of each component is critical in achieving an overall propulsion system which is both efficient and suited to the application platform's requirements.

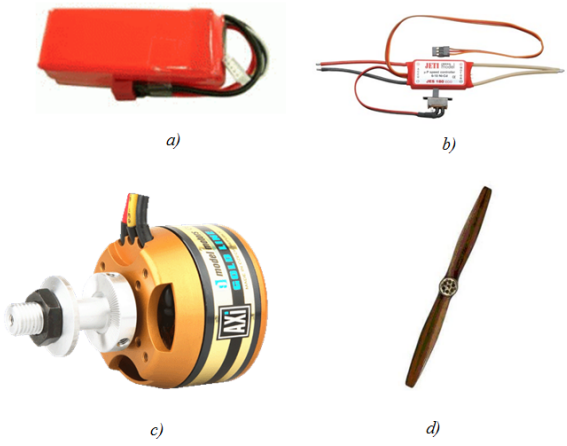

Fig. 1. Components of a typical electrical propulsion system. a) Battery, b) Electronic Speed Controller (ESC), c) Motor, d) Propeller.

The University of Johannesburg is currently developing a modular "Green Energy" UAV with power derived from batteries, solar power and a hydrogen fuel cell. In this paper, the investigation of a means of modelling, characterising and testing of brushless DC motors is presented. With a model that adequately represents BLDC motors, one can easily predict the characteristics of a given motor without the cost and time consuming loaded bench testing. The data gathered during this process aids in the selection of the remaining propulsion components needed for the UAV platform.

978-1-61284-993-5/11/$26.00 ©2011 IEEE

II. Theory Building and Methodology

A. Propulsion Power Transfer

The electric propulsion system converts electrical power to mechanical power in the form of thrust. Fig. 2 illustrates this power transfer through the four components of the propulsion system.

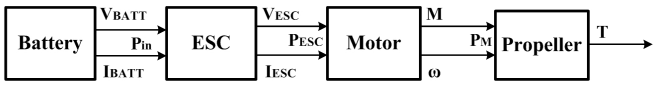

Fig. 2. Transfer of power through propulsion components.

The power derived from the battery source is given by (1):

$$P_{batt} = V_{batt} \times I_{batt} \tag{1}$$

Where:
V_{batt} Battery voltage [V]
I_{batt} Battery current [A]

The ESC receives Pulse Width Modulation (PWM) throttle control signals either from an on-board Radio Frequency (RF) receiver or an auto-pilot system. The percentage duty cycle depends on the required throttle position. The ESC controls the motor speed according to the percentage duty cycle. Power is transferred from the ESC to the motor in the form of a quasi-three-phase AC power architecture given by (2):

$$P_{ESC}(RMS) = V_{ESC}(RMS) \times I_{ESC}(RMS) \tag{2}$$

Where:
$V_{ESC}(RMS)$ ESC voltage [V]
$I_{ESC}(RMS)$ ESC current [A]

The brushless DC motor converts the electrical power to a torque (M) on its output shaft at a specific angular velocity (ω) given by (3):

$$P_M = M \times \omega \tag{3}$$

Where:
M Torque [N.m]
ω Angular velocity [rad/s]

The propeller converts the torque (M) and rotational speed to an aerodynamic thrust (T). The required thrust is determined from the UAV platform specifications. Selection of the correct electrical motor is essential for meeting the UAV platform application requirements.

B. Brushless DC Motor Theory

BLDC Configurations

Brushless DC motors eliminates the need for brushes used in shunt DC motors, thereby reducing maintenance costs. Instead, BLDC motors use electronic commutation through switching electronics to change the current direction. BLDC motors operate by means of stationary current-carrying coils and rotating permanent magnets [3]. Fig. 3 illustrates the two physical BDLC motor configurations — inner-rotor and outer-rotor. The inner-rotor places the magnets in the centre, surrounded by the coil windings. The outer-rotor places the coil windings enclosed by an outer casing composed of permanent magnets [4]. This configuration is favoured over the inner-rotor configuration in model aviation due to the need for lower energy magnets, reduced copper losses, reduced production costs, and greater rotor inertia [4].

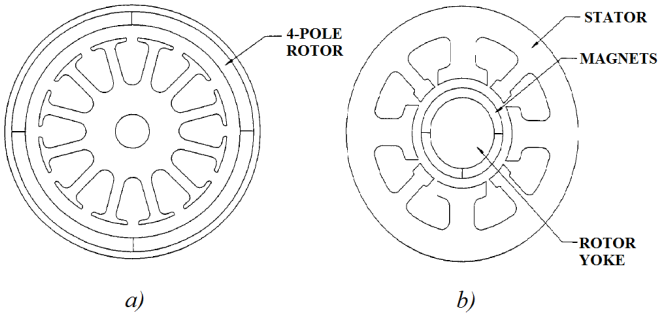

Fig. 3. The two BLDC motor configurations: a) Outer-rotor BLDC motor, b) Inner-rotor BLDC motor [4].

BLDC Stator Windings

The two most common types of winding configurations for 3-phase BLDC motors are Wye (Y) and Delta (Δ) — with their own advantages and disadvantages. Most commercial model aviation BLDC motors are Delta (Δ) wound and excel at high speed applications. Delta (Δ) wound motors have some disadvantages, these being: additional ohmic losses (over the Y configuration) and torque ripple from current circulation in the Delta loop [5].

The Y winding configuration is favoured for lower speed operation where greater torque production is needed. Y wound motors produce $\sqrt{3}$ more torque and $1/\sqrt{3}$ less rotational speed than Delta wound BLDC motors [5]. The relationship between Y and Δ windings can be represented by (4) and (5).

$$M_Y = \sqrt{3} M_\Delta \tag{4}$$

Where:
M Torque [N.m]

$$\omega_Y = \frac{1}{\sqrt{3}}\,\omega_\Delta \tag{5}$$

Where:
ω Angular velocity [rad/s]

C. BLDC Model

Most commercial "off-the shelf" BLDC motors used in UAV propulsion systems do not have available data with respect to the internal parameters of the motor - number of windings, core material, permanent magnet data etc. Modelling of these motors can be difficult as a result. A "black-box" parameter based model is needed. The most

common steady-state model used for BLDC motors is the three-constant model. The constants being: R_m, I_0, and K_v. R_m represents the motor winding resistance; I_0 the idle no-load current due to friction losses and magnetic hysteresis; and K_v the RPM per back-emf voltage [6].

The three-constant model falls short of adequately modelling all the losses of a BLDC motor [6]. The idle current (I_0) may increase according to the applied voltage, rather than remaining constant as predicted by the three-constant model. Eddy currents flow within the stator core due to the varying magnetic field from electronic commutation. Eddy currents losses are not accounted for in the three-constant model, these losses increase proportionally to the rate of change of magnetic flux according to Maxwell's equations i.e. rotational speed. Viscous damping (windage losses) are also neglected in this model — yet they can be substantial since windage power losses are quadratic in relation to the rotational speed of the motor.

The proposed model for BLDC motors consists of four constants — R_m, I_0, K_v and R_1. R_m is the combined ESC and winding resistance. I_0 differs from the three-constant model, now representing the no-load current at zero battery voltage [6]. K_v is identical to the three-constant model. The fourth constant, R_1, is used to model the Eddy current and viscous damping losses [6]. Fig. 4 is an electrical representation of the four-constant model for BLDC motors.

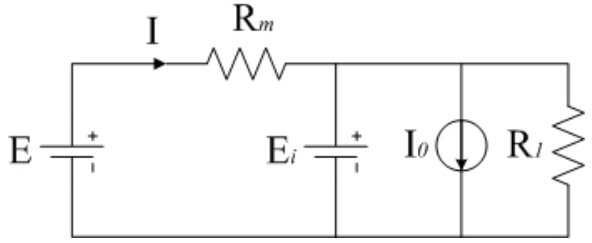

Fig. 4. Four-constant model for BLDC motors.

The electronic commutation is achieved by switch mode DC to AC converters in the form of what is commonly referred to as an Electronic Speed Controller. Switch mode converter losses are generally assigned to on-state, switching and energy storage medium losses. On state and energy storage losses are assumed linearly dependent on the current flowing through the converter. Switching losses are dependent on switching frequency and voltage by current during the cross over periods. Switching losses are greatly dependent on the rising and falling times of the switching architecture. The combined losses incurred by the ESC and the winding losses are represented by R_m in Fig. 4.

All four constants can be acquired by recording the no-load current and rotational speed in revolutions per minute (RPM) while varying the battery voltage (E). The R_m value is acquired from ESC and motor data sheets. Kirchhoff's voltage law is applied to the left-most loop of Fig. 4, which gives:

$$E_i = E - IR_m \tag{6}$$

Where:
- E_i Back-EMF [V]
- E Battery voltage [V]
- I Battery current [A]
- R_m Combined winding and ESC resistance [Ω]

The rotational speed of the motor is proportional to the back EMF (E_i) with, proportionality constant (K_v) given by:

$$K_v = \frac{N}{E_i} \tag{7}$$

Where:
- K_v RPM/Volt constant
- N Rotational speed of motor [RPM]
- E_i Back-EMF [V]

The value of I_0 can be obtained from the current axis interception of the battery current vs. battery voltage graph (I vs. E graph). The fourth constant (R_1) is obtained from the equation below:

$$R_1 = \frac{E - I(R_{esc} + R_m)}{I - I_0} \tag{8}$$

Where:
- R_1 Windage and Eddy current losses [Ω]

The power delivered to the load is calculated with (9):

$$P_{load} = \frac{E_i}{I_i} \tag{9}$$

Where:
- P_{load} Power delivered to load [Ω]
- I_i Load current [A]

The characteristic model prediction (efficiency vs. RPM) can be found using (1) and (9):

$$\eta = \frac{P_{load}}{P_{batt}} \times 100 \tag{10}$$

Where:
- η Efficiency [%]

D. Loaded Motor Characterisation

A loaded characterisation of BLDC is necessary in order to validate the four-constant model, and more importantly determine if a particular motor will satisfy the needs the UAV platform. A motor test bench is needed that has a stable means of mounting the motor under test; measurement of the output torque and RPM; and a means of increasing/decreasing the amount of mechanical loading on the motor. One such method is by means of a prony brake whereby, a pulley wheel (attached to the motor shaft) with a belt of fixed length connected at

978-1-61284-993-5/11/$26.00 ©2011 IEEE

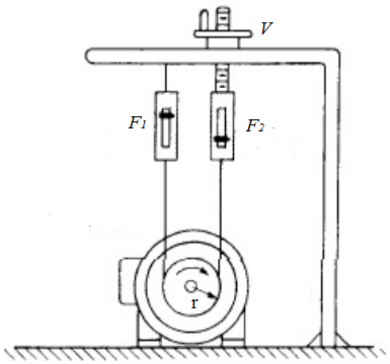

Fig. 5. Prony brake motor test setup [7].

each end to a load cell (Fig. 5). The motor load is increased by tightening the belt tension adjustment screw V in Fig. 5)

The difference of the two load cell forces (tangential to the pulley), together with the known pulley radius is used to calculate the output torque (11) [7]:

$$M = (F_1 - F_2)r \tag{11}$$

Where:

F_1	Force reading on load cell 1 [N.m]
F_2	Force reading on load cell 2 [N.m]
r	Pulley radius [m]

The pulley method is conceptually very basic, but hard to implement since there is slip between the belt and pulley, giving rise to noisy measurements on the load cells. The need for two load cells increases the cost of the experimental set-up.

A better experimental set-up is needed whereby experimental errors are minimised. The experimental set-up for loaded characterisation consists of two parallel uprights made of aluminium (Fig. 6). The BLDC motor under testing is mounted to the right-hand upright, which has been designed to slide towards/away from the left-hand upright in Fig. 6.

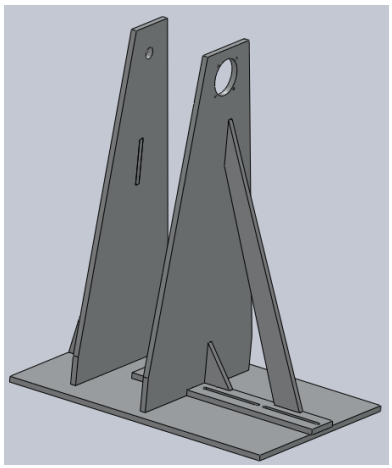

Fig. 6. Motor test bench.

The motor under test spins a 2 mm thick aluminium disk (300 mm diameter). The left-hand upright (Fig. 6) houses a freely rotating aluminium arm with two neodymium magnets at 120 mm from the pivot point of the arm. The rotating movement of the aluminium disk in close proximity to the rotating arm (housing magnets) induces Eddy currents to flow inside the aluminium disk. From Lenz's law, these Eddy currents will flow in such a manner as to oppose the change in flux, causing the arm to rotate opposite to that of the disk.

The force at a displacement of 500 mm from the pivot of the arm is measured with a load cell. Rotational speed of the motor is measured via a hall or optical sensor. The torque and power output of the motor can be calculated from (12) and (13) respectively.

$$M_{arm} = F_{loadcell} \times r \tag{12}$$

Where:

M_{arm}	Torque [N.m]
$F_{loadcell}$	Force[N]
r	Displacement [m]

$$P_{arm} = M_{arm}\omega \tag{13}$$

Where:

P_{arm}	Power [W]
M_{arm}	Torque [N.m]
ω	Angular velocity [rad/s]

Bringing the motor upright towards/away from the rotating arm will increase/decrease the load to the motor under test respectively. There is a power loss incurred due to the viscous damping from the aluminium disc spinning in air which, needs to be accounted for using a quadratic fitting to the no-load current vs. voltage plot with the aluminium disk attached to the motor shaft (14).

$$P_{disk} \propto \omega \tag{14}$$

From (13) and (14), the output power from the BLDC motor under test is:

$$P_M = P_{arm} + P_{disk} \tag{15}$$

The motor efficiency is:

$$\eta = \frac{P_M}{P_{batt}} \times 100 \tag{16}$$

III. Results and Discussions

The motor characterisation was performed to ascertain which motor would meet the requirements of the given UAV platform. The requirements for the motor where: operate at maximum efficiency above 80 % and provide a minimum of 0.5 N.m of torque at 6 A battery current — whilst supplied by a 4-cell 14.8 V Lithium Polymer (LiPo) battery pack. Three BLDC motors were tested and characterised using the four constant model predictions and loaded testing. The following motors were tested:

978-1-61284-993-5/11/$26.00 ©2011 IEEE

1) Scorpion S5525(Δ);
2) Scorpion S5525(Y);
3) Axi 5320/34(Δ);

The no-load I vs. V plots for the Scorpion S5525(Δ), Scorpion S5525(Y), and Axi 5320/34 (Δ) allows for extraction of the I_0 and R_1 constants (Fig. 7). Analysing the plots one can see the idle current at zero battery voltage (I_0) for all three motors tested i.e. the I-axis intercepts. The Scorpion S5525 (Y) therefore has the lowest hysteresis and friction losses (see Section II-C), followed by the Axi 5320/34(Δ) and the Scorpion S5525(Δ). The K_v and R_1 constants are found using (7) and (8) respectively. The slope of each plot from Fig. 7 gives us insight into the R_1 eddy current and windage losses (see Section II-C), i.e. the steeper the slope gradient — the lower the R_1 value.

The constants from no-load testing are presented below in Table I. Note the Scorpion S5525 motor was tested in both Y and Δ winding configurations, where the Y K_v constant is approximately $\sqrt{3}$ times larger than the equivalent Δ connected motor (as predicted from Section II-B).

TABLE I
NO-LOAD MOTOR CONSTANTS.

Motor	K_v	$R_m(\Omega)$	$I_0(A)$	$R_1(\Omega)$
Scorpion S5525(Δ)	180	0.125	0.982	19.443
Scorpion S5525(Y)	104	0.16	0.474	52.140
Axi 5320/34(Δ)	220	0.14	0.511	85.608

The constants in Table I were used to predict each motor's efficiency vs. current curve. This is illustrated for the Scorpion S5525 Δ, Scorpion S5525 Y, and Axi 5320/34 Y in Fig. 8.

Validation of these prediction results was done by means the motor test bench as shown in Fig. 6. Input voltage, current and power measurements were taken using a Yokogawa 2533 Digital power meter. Force and RPM measurement were obtained by means of a load cell and hall sensor respectively. Output power measurement was obtained through equations 11, 12, 13 & 14, with efficiency from (15). Each motor was tested over its intended operating load region with a constant 14.8V DC power supply source. The predicted plots follow the results from loaded testing accurately, proving that the four-constant model for BLDC motors can be used with confidence when selecting a motor for a UAV platform.

The Scorpion S5525(Δ) motor produced 0.64 N.m of torque and reached a maximum efficiency of 79 % @ 14 A — making it unsuitable for the UAV platform requirements due to the high operating current and low efficiency. The Axi 5320/34(Δ) produced 0.46 N.m of torque at an efficiency of 82.2 % @ 6 A. At the required operating current (6 A), the Scorpion S5525(Y) produced 0.52 N.m of torque with an efficiency of 82 % — meeting the requirement of above 80 % efficiency. The fact that the Scorpion S5525(Y) reaches an even higher efficiency of 84.4 % @ 7.5 A, indicates the motor is very efficient — should the motor load increase due to flight conditions or additional UAV payload.

IV. CONCLUSION

The UAV industry has grown into a multi-billion dollar, highly competitive market. It is of paramount importance to each UAV manufacturer to provide a UAV capable of sustaining level flight for very long durations. Apart from the UAV platform's aerodynamic design, the propulsion system becomes the largest system that restricts long endurance flight. In this paper a means of modelling, bench testing and characterising brushless DC motors (BLDC) has been presented. Knowing the characteristics of a BLDC motor aids in the design of the additional components — in the quest for an efficiently integrated propulsion system.

Modelling of a BLDC motor becomes difficult without knowing the internal parameters of the motor. The four-constant model provides a relatively easy, yet effective means of predicting a specific motor's performance capabilities — reducing the need for time consuming loaded bench testing. This is validated against physical loaded bench testing of each motor.

Three typical production grade motors were tested, two of which were identical apart from winding connection (Scorpion S5525(Δ) and S5525(Y)). The findings were that Scorpion S5525(Δ) (low efficiency) and the Axi 5320/34(Δ) (low torque) were not suitable for the UAV platform requirements (see Section III). The Scorpion S5525(Y) motor was chosen since it reached higher efficiencies over and above the required operating current, while providing sufficient torque.

REFERENCES

[1] tealgroup.com, "Teal group predicts worldwide uav market will total over $80 billion in its just released 2010 uav market profile and forecast," Internet Page, Accessed March 2011. [Online]. Available: http://www.tealgroup.com/index.php?option=com_content&view=article&id=62:uav-study-release&catid=3&Itemid=16
[2] C. Herwerth, U. Ofoma, C. Wu, S. Matsuyama, and S. Clark, "Development of a fuel cell powered uav for environmental research," in *Proc. 44th AIAA Aerospace Sciences Meeting and Exhibit*, Reno, Nevada, Jan. 2006, pp. 2006–237.
[3] A. Emadi, *Handbook of automotive power electronics and motor drives*, A. Emadi, Ed. Florida, United States of America: CRC Press, 2005.
[4] W. H. Yeadon, *Handbook of small electric motors*, W. H. Yeadon, Ed. United States of America: McGraw-Hill, 2001.
[5] D. C. Hanselman, *Brushless permanent-magnet motor design*, H. B. Crawford, Ed. United States of America: McGraw-Hill, 1994.
[6] J. Carri. (2007) A four-constant model for electric motors (draft no. 2). Internet draft. [Online]. Available: http://flbeagle.rchomepage.com/research/4_consts_paper_ver_02.pdf
[7] T. Wildi, *Electrical Machines, Drives, and Power Systems*, 6th ed., A. Wolf, Ed. United States of America: Prentice Hall, 2006.

978-1-61284-993-5/11/$26.00 ©2011 IEEE

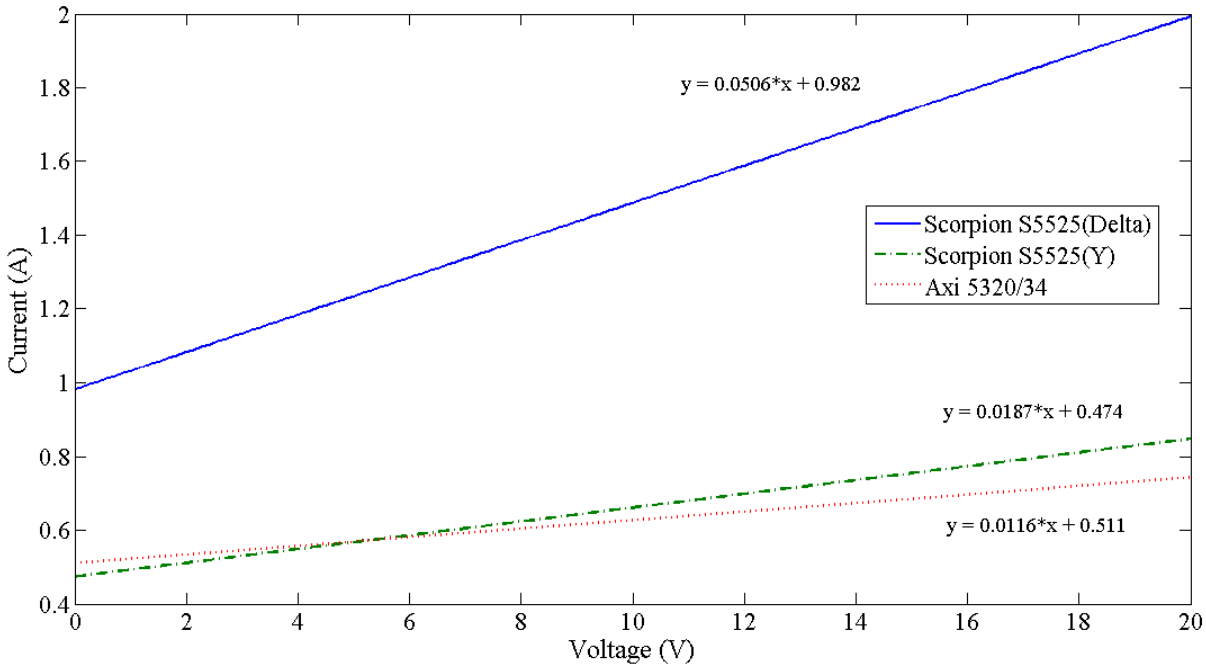

Fig. 7. No-load battery current vs. battery voltage for Scorpion S5525(Δ), Scorpion S5525(Y) and Axi 5320/34(Δ).

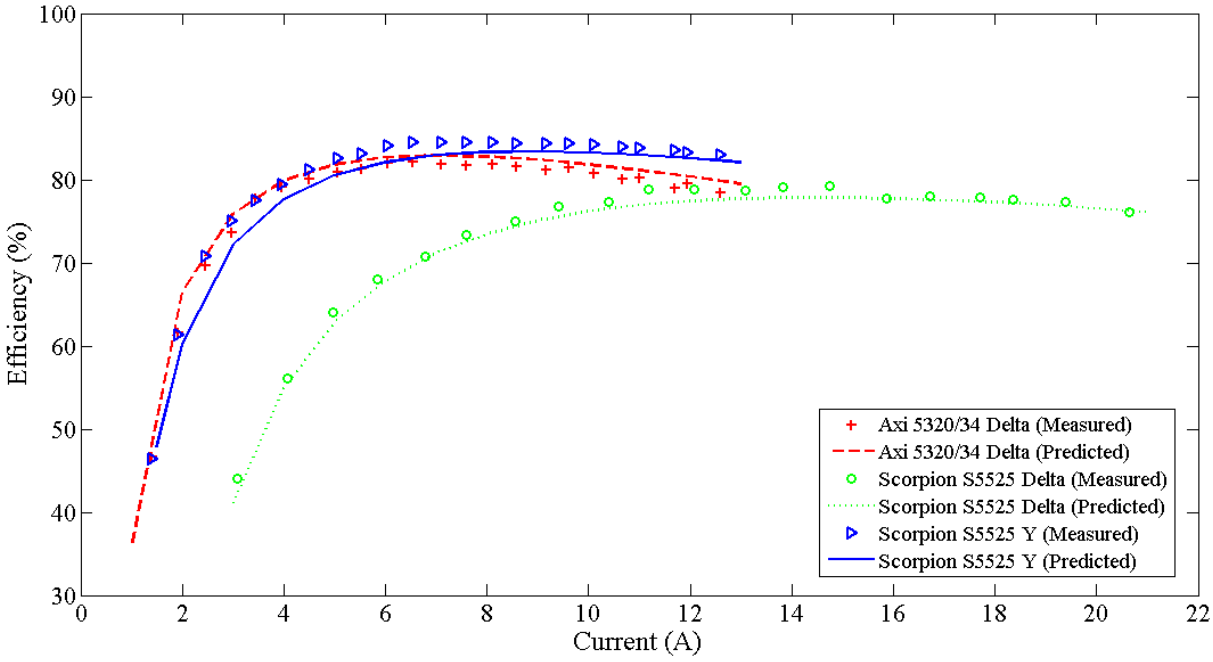

Fig. 8. Loaded efficiency vs. battery current for Scorpion S5525(Δ), Scorpion S5525(Y) and Axi 5320/34(Δ).

978-1-61284-993-5/11/$26.00 ©2011 IEEE